Lack of the transcription factor hypoxia-inducible factor (HIF)-1α in macrophages accelerates the necrosis of *Mycobacterium avium*-induced granulomas

Marcos S. Cardoso[1], Tânia M. Silva[1,2], Mariana Resende[1, 2, 3, 4], Rui Appelberg[1, 2, #] and Margarida Borges[1, 5, #]

IBMC– Instituto de Biologia Molecular e celular, Universidade do Porto, 4150-180, Porto, Portugal[1]; Instituto de Investigação e Inovação em Saúde, Universidade do Porto, 4200, Porto, Portugal[2]; Life and Health Sciences Research Institute (ICVS), School of Health Sciences, University of Minho, 4710-057, Braga, Portugal[3]; ICVS/3B's – PT Government Associate Laboratory, 4710-057, Braga, Portugal[4]; UCIBIO/REQUIMTE, Departamento de Ciências Biológicas, Laboratório de Bioquímica, Faculdade de Farmácia da Universidade do Porto, 4050-313, Porto, Portugal[5].

Running Title: HIF-1α in mycobacterial immunopathology

#Corresponding authors:
Rui Appelberg, rappelb@ibmc.up.pt
Margarida Borges, mborges@ff.up.pt

Abstract

The establishment of mycobacterial infection is characterized by the formation of granulomas, which are well-organized aggregates of immune cells, namely infected macrophages. The granuloma's main function is to constrain and prevent dissemination of the mycobacteria, while focusing the immune response to a limited area. In some cases these lesions can grow progressively into large granulomas which can undergo central necrosis, thereby leading to their caseation. Macrophages are the most abundant cells present in the granuloma and are known to adapt under hypoxic conditions in order to avoid cell death. Our laboratory has developed a granuloma necrosis model that mimics the human pathology of *Mycobacterium tuberculosis*, using C57BL/6 mice infected intravenously with a low dose of a highly virulent strain of *Mycobacterium avium*. In this work, a mouse strain deleted of the hypoxia inducible factor (HIF)-1α under the Cre-lox system regulated by the Lysozyme M gene promoter was used to determine the relevance of HIF-1α in the caseation of granulomas. Genetic ablation of HIF-1α in the myeloid lineage causes the earlier emergence of granuloma necrosis and clearly induces an impairment of the resistance against *M. avium* infection coincident with the emergence of necrosis. The data provide evidence that granulomas become hypoxic before undergoing necrosis, through the analysis of vascularization and quantification of HIF-1α in a necrotizing mouse model. Our results show that interfering with macrophage adaptation to hypoxia, such as through HIF-1α inactivation accelerates granuloma necrosis.

Keywords: hypoxia, macrophages, granuloma, mycobacteria.

Introduction

The main pathologic feature of human tuberculosis is the induction by *Mycobacterium tuberculosis* of granulomas which undergo central necrosis (caseous necrosis) (1). The mechanisms underlying the latter phenomenon are not clear but it is generally accepted that caseation plays an essential role in the pathogenesis and dissemination of the infection. Caseous necrosis and cavitation during infection by *M. tuberculosis* is more prominent in rabbits and guinea pigs than in mice (2). Nevertheless, human-like pathology, as central granuloma necrosis and associated hypoxia, can be obtained in *M. tuberculosis*-infected I/StSnEgYCit, C3HeB/FeJ or IL13-over-expressing C57Bl/6 mouse strains (3-5). Confluent necrotic granulomas are also observed in mice deficient in gamma interferon (IFN-γ) or the type 1 tumor necrosis factor (TNF) receptor (2, 6, 7). However, the fact that immunodeficient human hosts, namely AIDS patients, tend to present forms of tuberculosis with granulomas lacking necrotic features suggests that necrosis depends on the immune response (8).

We have shown that mice infected with a small inoculum of *M. avium* ATCC 25291 establish a chronic and progressive infection characterized by the formation of discrete granulomas, which gradually increase in size and undergo central necrosis within a few months (9). This requires $CD4^+$ T cells as well as an intact interleukin (IL)-12/IFN-γ cytokine axis (9) but is independent of the generation of toxic mediators induced by IFN-γ in macrophages, such as the products of the inducible (type 2) nitric oxide synthase (iNOS) or the phagocyte NADPH oxidase (NOX2) (9). Granuloma necrosis also occurs in mice with genetic ablation of death receptors, such as type 1 TNF receptor or Fas (CD95) or the TNF superfamily members TNF or TNF-related apoptosis inducing ligand (TRAIL) (9-11). On the other hand, granuloma

73 necrosis is not observed in certain inbred strains of mice such as BALB/c or DBA/1.
74 In the former strain, this was due to the increased production of the anti-inflammatory
75 cytokine IL-10 (12). In the latter, it was related to the inability to form large
76 granulomas due to the lack of the complement component C5 (12).
77 Granuloma necrosis does not occur when these lesions fail to grow to the size
78 observed in C57Bl/6 mice, such as in animals lacking T cells altogether or, more
79 specifically, $CD4^+$ T cells, in animals with reduced or no IFN-γ production, as well as
80 in the DBA/1 strain (9). Interestingly, infection of immunocompetent C57BL/6 mice
81 with a high dose of the same *M. avium* strain did not induce necrotic granulomas. The
82 explanation for this result lies in the fact that in this type of infection severe
83 lymphopenia is induced and granulomas do not get to be as large as those observed
84 when T cells are spared, i.e. in low dose infections (13).
85 Granulomas are believed to be poorly vascularized structures and thus there may be a
86 difficulty in providing nutrients and oxygen to the cells, in particular to those at the
87 core of the lesion in bigger lesions. It is therefore fair to hypothesize that nutrient
88 deprivation and/or hypoxia may underlie the genesis of granuloma necrosis. Given
89 that macrophages are the most abundant cells at the center of the granuloma these
90 might be the cells that die. Yet, macrophages are known to adapt to hypoxic
91 conditions namely by using the glycolytic pathway to generate ATP (14). Central to
92 these metabolic adaptations is the transcription factor hypoxia inducible factor (HIF)-
93 1α.
94 HIF-1α is directly involved in angiogenesis (15), erythropoiesis (16), cell growth and
95 differentiation (17), survival and apoptosis (18). Under normoxic conditions, HIF-1α
96 has a very short half-life, being suppressed by hydroxylation of two prolyl residues
97 (Pro-402 and Pro-564). This modification allows the interaction with the von Hippel-

Lindau tumor suppressor protein (pVHL), the recognition component of an E3 ubiquitin ligase complex that targets HIF-1α for ubiquitination and proteasomal degradation. Under hypoxic conditions, prolyl hydroxylation is suppressed and HIF-1α escapes from proteasomal degradation becoming stable and translocating from the cytoplasm to the nucleus where it dimerizes with HIF-1β. The HIF complex formed becomes transcriptionally active, binding hypoxia-response elements (HREs) (19, 20). Classical HIF-1α target genes include the vascular endothelial growth factor (21), erythropoietin (16), glucose transporters (22) and transferrin (23). The influence of HIF-1α in the innate immune system is relatively well established and recently its role in adaptive immune responses is being recognized (24, 25).

Mice lacking HIF-1α in cells from the myeloid lineage show impairment of myeloid cell functions (25) whereas HIF-1α activation increased their activity under hypoxic conditions (26). HIF-1α is strongly stimulated upon exposure to bacteria and has the ability to regulate the production of nitric oxide (NO) and TNFα by phagocytes (27). HIF-1α also plays a role in T cells (28), B cells (29), neutrophils (30), or dendritic cells (31, 32), and regulates the differentiation of Th17 cells and regulatory T cells (33, 34) and the production of pro-inflammatory cytokines in response to T cell receptor activation (28). Non-hypoxic stimuli such as glucose concentrations (35), lipopolysaccharide (LPS) (36), interferons (37), TNF-α (38) and nuclear factor (NF)-κB (39) are additional modulators of HIF-1α transcription and, therefore, are able to influence the expression of hypoxic genes.

Here we found that the genetic ablation of HIF-1α in the myeloid lineage causes the earlier emergence of granuloma necrosis during low dose infection by virulent *M. avium*. These data support the view that hypoxia is one of the causes for granuloma

122 necrosis and that interfering with the adaptation of macrophages to this condition
123 exacerbates this type of pathology.
124

Materials and Methods

Mice, bacteria and infection

C57Bl/6 wild-type mice (WT) were bred in our facilities from a breeding pair purchased from Harlan Iberica (Barcelona, Spain). C57Bl/6 mice with a myeloid deficiency in HIF-1α (HIF-1$\alpha^{-/-}$) were obtained in our facilities after back-crossing the C57BL/6.129-Hif1$\alpha^{tm3RSjo}$/J and the C57BL/6.129P2-Lyz2$^{tm1(cre)Ifo}$/J strains, from the Jackson Laboratory (Bar Harbor, ME, USA). The genotyping was performed according Jackson Laboratory protocols (Bar Harbor, ME, USA). All mice were kept in our animal facilities in high-efficiency particular air (HEPA)-filter-bearing cages under 12h light cycles, and fed autoclaved chow and water *ad libitum*. Experimental mice were age- and sex-matched and used between the ages of 8 and 12 weeks. The highly virulent *Mycobacterium avium* strain 25291 (ATCC 25291 SmT) was obtained from the American Type Culture Collection (Manassas, VA, USA). Bacterial inocula were prepared as described previously(40). Mice were infected with 10^2CFU of *M. avium* strain 25291 through a lateral tail vein. The bacterial load in the organs was determined as previously described(40). All animal experiments were performed in accordance with the recommendations of the European Convention for the Protection of Vertebrate Animals Used for Experimental and Other Scientific Purposes (ETS 123) and 86/609/EEC Directive and Portuguese rules (DL 129/92). The animal experimental protocol was approved by the competent national authority Direção Geral de Veterinária.

Liver mononuclear cell isolation

Liver samples were collected in Dulbecco's modified Eagle's tissue culture medium (DMEM; Life Technologies, Paisley, UK) containing 10% fetal bovine serum (FBS; Life Technologies), 5% glutamine and 1% penicillin/streptomycin (P/S) and

processed individually. A single cell suspension was obtained by passing the liver through a 70µm cell strainer (BD Biosciences, San Jose, CA, USA). Cells were washed with phosphate-buffered saline (PBS) until the supernatant got clear, resuspended in DMEM and subjected to density centrifugation using Histopaque 1083 (Sigma-Aldrich, St Louis, MO, USA). After centrifugation at 1000g for 25min at room temperature (RT) without acceleration or brake, liver mononuclear cells were recovered, washed resuspended in DMEM and the number of viable cells was counted by trypan blue exclusion using a haemocytometer.

HIF-1α quantification

Liver mononuclear cells were fractionated into cytoplasmic and nuclear protein extracts using a cell fractionation kit according to the manufacturer's instructions (BioVision, Mountain View, CA, USA). Total HIF-1α was quantified using the cytoplasmic extracts by a two-site enzyme-linked immunosorbent assay (ELISA) according to the manufacturer's instructions (R&D Systems, Minneapolis, MN, USA). Positive controls were provided by the manufacturer. All samples were assayed in duplicate. The values were normalized to the total liver mononuclear cell number isolated from each mouse.

Flow cytometry

For the immunofluorescence staining, 10^6 cells were labeled with distinct combinations of the following antibodies (Abs): fluorescein isothiocyanate (FITC)–conjugated anti-CD19, phycoerythrin (PE)–conjugated anti-CD3, V450–conjugated anti-CD4 and V500–conjugated anti-CD8, brilliant violet 510 (BV 510)–conjugated anti-CD11b, BV 421–conjugated anti-CD11c, allophycocyanin (APC)–conjugated anti-Ly6G, APC with cyanin-7 (APC/Cy7)–conjugated anti-F4/80. All the Abs were obtained from Biolegend (San Diego, CA, USA) except V450-CD4 and V500-CD8

that were obtained from BD Biosciences (San Jose, CA, USA). The acquisition of cells was performed using a FACS Canto II flow cytometer using BD FACSDiva software (BD Biosciences). Data were analyzed using FlowJo software (Tree Star, Ashland, OR). Cells were selected on the basis of FSC/SSC and the singlets were gated according to size *versus* width. For the lymphocyte analysis we used CD19 as a marker of B cells and CD3, CD4 and CD8 to label T cells. $CD11b^{+}Ly6G^{high}$ were defined as neutrophils. $CD11b^{+}Ly6G^{-}F4/80^{+}$ and $CD11b^{+}/Ly6G^{-}/CD11c^{high}$ were defined as macrophages and DCs, respectively. To determine the cell number, the number of gated events for each cell population was multiplied by the total cell number (counted using Kova chambers) and divided by the total number of events select by FSC/SSC parameters.

Histology and morphometric analysis of the granulomatous area

Portions of the livers were fixed in buffered formaldehyde and embedded in paraffin. Sections (4 µm) were stained with haematoxylin and eosin (H&E). Slides were photographed using an Olympus CX31 light microscope equipped with a DP-25 camera (Imaging Software CellˆB, Olympus, Center Valley, PA, USA). One liver section per animal with random fields selected in a blind way was analyzed. Granulomatous infiltration necrotic and non-necrotic areas determination was done in a total tissue area ranging from 6 to $9x10^{6}$ μm^{2}, corresponding to six fields analyzed in each section. To determine the liver area covered by granulomas, the NIH ImageJ software program was used. The percentage of granuloma area was calculated for each mouse by dividing the sum of granulomatous areas by the total area of the liver section analyzed. The number of cellular infiltrates was the sum of all granulomatous/cell infiltration areas.

Immunohistochemistry

Paraffin sections were dewaxed, re-hydrated and permeabilized in PBS containing 0.1% Triton X-100 and 0.1% Tween. After antigen retrieval with 10mM sodium citrate buffer for 30min at 96ºC, endogenous peroxidase activity was blocked with 0.3% hydrogen peroxidase in methanol for 35min at RT, followed by blocking the nonspecific Ab binding with normal horse serum (Vector Labs, Burlingame, CA, USA). Sections were incubated overnight at 4ºC with rat IgG monoclonal anti-mouse F4/80 (Clone Cl:A3-1; Abcam) or rat IgG monoclonal anti-mouse Endomucin (Clone V.7C/.1; Abcam). After washing with PBS, sections were incubated with goat anti-rat IgG, horseradish peroxidase conjugated Ab (GE Healthcare). Development was performed with 3,3-diaminobenzidine (DAB) labeling system (Vector Labs). Sections were then counterstained with Gill's hematoxylin, dehydrated and mounted in DPX (Sigma-Aldrich).

Immunofluorescence

Paraffin sections were dewaxed, re-hydrated and permeabilized in PBS containing 0.1% Triton X-100 and 0.1% Tween. After antigen retrieval with 10mM sodium citrate buffer for 30min at 96ºC, nonspecific Ab binding was block with 5% BSA in PBS, 0.1% Triton X-100, 0.1% Tween. Sections were incubated for 3h at RT with rabbit IgG monoclonal anti-human/mouse active Caspase 3 (R&D Systems). After washing with PBS, sections were incubated with goat anti-rabbit IgG, Alexa Fluor 488 conjugated Ab (Life Technologies). Sections were then counterstained and mounted with DAPI-vectashield and were observed using a Zeiss Imager Z1 microscope.

Terminal deoxynucleotidyl transferase dUTP nick end labelling (TUNEL) assay

Paraffin sections were dewaxed, re-hydrated, permeabilized in 0.1% Triton X-100, 0.1% sodium citrate for 8min at RT and washed twice with PBS. Nicked DNA was labelled by incubating the cells with the label solution containing fluorescein-2′-deoxyuridine 5′-triphosphate (dUTP) and terminal deoxynucleotidyl transferase (TdT) (Roche Diagnostics, Penzberg, Germany) for 1h at 37°C in a humidified atmosphere in the dark. Negative and positive controls were performed by incubating the slides without TdT and recombinant DNase I (Roche) in 50mM Tris-HCl, pH 7.5, 10mM $MgCl_2$, 1mg/ml BSA for 10min at RT, respectively. Sections were counterstained and mounted with DAPI-vectashield and were observed using a Zeiss Imager Z1 microscope.

In vitro stimulation of spleen cells and IFNγ quantification

Spleen cell suspensions were processed individually as described previously(10). Cells were cultivated at a density of $2x10^5$ cells/well in a U-bottom 96-well microtitre plate and incubated in triplicate in DMEM with 10% FCS with no stimulus or stimulated with mycobacterial envelope proteins (4µg/ml). Supernatants from the cultures were collected after 72h of culture at 37ºC in a 7% CO_2 incubator and the IFN-γ produced was quantified by the ELISA method using anti-IFN-γ-specific affinity-purified mAb (R4-6A2 as capture and biotinylated AN-18 as detecting Ab). A standard curve was generated with known amounts of recombinant murine IFN-γ (Genzyme, Cambridge, CA, USA). The OD were recorded at 450nm.

Infection of Bone Marrow Macrophages and treatments

Macrophages from WT and HIF-$1\alpha^{-/-}$ mice were obtained as described previously (41). Recombinant murine IFN-γ (Gibco), 100U per culture well and recombinant murine TNF-α (Genzyme), 50U per culture well, were added daily to the cultures, starting immediately after infection and until day 7.

Statistics

Results were expressed as mean + SD. Statistical significance was calculated by using the unpaired Student *t*-test for data presented on Figures 3 and 4 and the one-way ANOVA test with a Tukey's post-test for data presented in Figure 5. The *p* values <0.05 were considered statistically significant.

Results

Evolution of the granuloma induced by *M. avium*

WT mice were infected with a low dose of *M. avium* and liver histological sections were analyzed at different time-points of infection. Liver was selected as it is the organ where most of the inoculum is implanted following intravenous infection and where the delineation of the granuloma from the surrounding tissue is easier. To assess the cellular constitution of the granuloma we stained macrophages by immunohistochemistry (IHC), using F4/80-specific antibodies (42). As shown in Figure 1, granulomas from day 30 to day 120 post-infection were mostly constituted by macrophages forming granulomas of progressively bigger size. Caseating granulomas (Fig. 1D) had the necrotic center surrounded by F4/80 positive cells.

It has been described that caseating granulomas show signs of hypoxia in the necrotic areas (43), raising the possibility that hypoxia is common in the granulomatous environment. In fact, granulomas are considered to be poorly vascularized structures and the limited blood supply could cause a reduction in nutrient and oxygen supply at the core of the granuloma (43). Alternatively, hypoxia could simply reflect the destruction of the integrity of the tissue and be a consequence rather than a cause the granuloma necrosis. We thus analyzed vascularization during granuloma development by the immunohistochemical detection of endomucin (44). As shown in Figure 2, small granulomas show an extensive vascular bed and preservation of cellular integrity (Fig. 2A) but, as they increase in size, signs of cellular decay with accumulation of neutrophils can be seen in areas with a smaller density of blood vessels (Fig. 2B). At advanced stages, granulomas show large areas of necrosis and no evidence of vascularization except at the periphery of the granuloma where cells are

still intact (Fig. 2C, D). These data indicate that macrophages at the center of granulomas with poor vascularization may die due to reduced access to nutrients and/or oxygen.

Evidence for the development of hypoxia in the tissues of infected mice

Necrotic areas in *M. tuberculosis* or *M. avium* granulomas are hypoxic (43, 45, 46). Our observations showed that small non-necrotic granulomas were well vascularized structures, but as granulomas enlarged the central core became less vascularized. This could be responsible for a decrease in oxygen supply and thus lead to a hypoxic environment. Since HIF-1α is an important regulator of hypoxia (19, 20), we evaluated HIF-1α protein content in liver mononuclear cells during *M. avium* infection. We found a significant increase of total HIF-1α protein levels in cells from infected animals as compared with the non-infected animals beginning at day 60 post-infection (Fig. 3A). These results indicate HIF-1α accumulation at the onset of granuloma necrosis (60 and 90 days post- infection).

Consequences of a myeloid HIF-1α deficiency

The stabilization of HIF-1α and the consequent activation of a targeted transcriptional program allow cells to adapt to hypoxia (20). In the absence of HIF-1α it is expectable that cells fair less well in hypoxic environments and die. In a preliminary assessment of the impact of myeloid deficiency in HIF-1α on the course of *M. avium* infection *in vivo*, we infected HIF-1$\alpha^{-/-}$ and WT mice with a low dose (100 CFU) of *M. avium* 25291. Mice were sacrificed at different time-points post-infection and their organs analyzed. Infected mutant mice exhibited increased organ sizes and macroscopic tubercles at 96 days of infection (Fig. 3B and C). The bacterial burdens

in the spleen and liver were also increased in mutant as compared to WT mice (Fig. 3D). Importantly, the exacerbation of bacterial growth occurred late in infection with no differences in the replication of *M. avium* during the first month of infection in the spleen and in the first two months of infection in the liver.

Impact of myeloid HIF-1α deficiency on granuloma integrity and macrophage apoptosis/necrosis

We studied the evolution of the granulomas in both strains by analyzing H&E stained liver sections. At day 30 post-infection, lesions of both HIF-1$\alpha^{-/-}$ and WT mice were very small and incipient (Fig.4A and D). After day 60 post-infection, differences between the lesions in either strain were evident, showing initial necrosis of granulomas in HIF-1$\alpha^{-/-}$ mice and smaller granulomas still lacking signs of necrosis in WT animals (Fig. 4B and E). At day 104 of infection, extensive granuloma necrosis was found in all HIF-1$\alpha^{-/-}$ mice analyzed and in none of the WT animals analyzed. We quantified the type of pathology in the liver by distinguishing necrotic from non-necrotic areas within the infiltrates. Morphometric analysis determining the infiltrated necrotic or non-necrotic areas confirmed the importance of HIF-1α in the evolution of the granuloma. No differences in liver inflammatory infiltrates were found at day 30 post-infection between the two mouse strains. At day 60 post-infection, a slight albeit not statistically significant increase in inflammatory area was observed in HIF-1$\alpha^{-/-}$ mice as compared with WT mice. On day 104 post-infection, the organs of HIF-1$\alpha^{-/-}$ mice showed a marked and statistically significant increase in inflammatory areas (Fig. 4G) and number of lesions (Fig. 4H) as compared to WT mice. More important, a large fraction of the inflammatory lesions in HIF-1$\alpha^{-/-}$ mice was constituted of necrotic material whereas no necrosis was yet found in WT mice. The development of

necrosis in liver granulomas was coincident with the increase in bacterial numbers (Fig. 3D). These results show that the lack of HIF-1α in myeloid cells anticipates the emergence of necrosis, augments the extent of inflammation and increases the susceptibility to infection. In order to determine the molecular mechanism underlying granuloma necrosis in the absence of HIF-1α we performed the TUNEL assay and detected caspase-3 activation by immunofluorescence in liver sections of organs from HIF-1α-deficient animals presenting necrotic lesions. On day 104 post-infection, the granulomas of HIF-1α$^{-/-}$ mice showed cleaved caspase-3 positive cells and marked internucleosomal DNA fragmentation at the center of the lesions demonstrating that cell demise within a granuloma occurs by apoptosis followed by secondary necrosis (Fig. 5). Granuloma evolution, vascularization and bacterial load were also evaluated in the lungs. The histological observation of the organ at the longest time points showed small lesions without signs of necrosis, comparable granuloma vascularization and no differences in bacterial burden in both strains of mice. Further morphometric analysis indicated no differences in infiltrated area or in the number of lung inflammatory infiltrates from HIF-1α$^{-/-}$ and WT mice (Fig S1).

The immune response in the absence of myeloid HIF-1α

Given the involvement of HIF-1α in the adaptive immune response, we assessed cellular responses in the liver as well as in the spleen. The number of macrophages, DCs and neutrophils in the spleen remained low until day 60 of infection in both strains but increased by day 104 of infection with significantly higher numbers of these cells in mutant mice as compared to the WT animals (Fig. 6A). Similar findings were obtained for macrophages and DCs in the liver (Fig. 6B). However, neutrophils could not be quantified given the isolation procedure employed which does not allow

the recovery of this cell type. The analysis of spleen lymphocyte populations revealed no significant differences at day 60 post-infection, as previously shown (9). However, at the late time-point of infection analyzed, a significant increase of $CD4^+$ and $CD8^+$ cell populations were observed in HIF-$1\alpha^{-/-}$ mice compared to WT mice (Fig. 6A). A significant increase in the number of splenic $CD19^+$ cells was found in both infected mouse strains compared to the respective non-infected strains (Fig. 6A). The analysis of liver lymphocyte populations indicated no differences for $CD4^+$ or $CD8^+$ lymphocytes at the time-points analyzed (Fig. 6B). A significant increase in$CD19^+$cells in the liver was observed in infected WT compared to HIF-$1\alpha^{-/-}$ mice suggesting a higher accumulation of B cells in the liver in the presence of HIF-1α (Fig. 6B).

Spleen cells from mutant mice infected for 99 days secreted similar amounts of IFN-γ as cells from wild type animals (26.9±3.8pg/ml *versus* 27.3±1.6pg/ml, respectively) in response to *M. avium* antigen. Thus, T cells appear to respond similarly to *M. avium* in either strain (data not shown).

Given that the physiology of the macrophage itself might be affected by the absence of HIF-1α, we performed *in vitro* infections of bone marrow-derived macrophages that were activated or not by a combination of IFN-γ plus TNF-α. Bacteria proliferation in non-activated macrophages was similar in mutant and WT cells (1.08 *versus* 1.20 $\log_{10}$ increase in CFU in 7 days, respectively). Activation of macrophages with cytokines led to a similar reduction in *M. avium* growth in either mutant or WT cells (0.70 *versus* 0.83 $\log_{10}$ increase in CFU in 7 days, respectively). Nevertheless, macrophages from mutant mice appeared to control the mycobacteria as well as WT cells, at least under normoxic conditions (data not shown).

Discussion

Much has already been learnt about the cellular and molecular mechanisms underlying the structuring of the mycobacterial granuloma, but the mechanisms specifically leading to granuloma necrosis are still poorly understood. We have shown in a mouse model of *M. avium* infection that this process is highly dependent on $CD4^+$ T cells, IFN-γ, and IL-12, and partly on IL-6 and CD40 (9, 47). Recently, it has been described that necrotic granulomas developed in *M. tuberculosis*-infected guinea pigs, rabbits and nonhuman primates (45), as well as in *M. avium* (strain TMC724)-infected WT mice are hypoxic(43). In this work we tested the hypothesis that hypoxia may underlie the origin of granuloma necrosis. We have used WT mice infected with *M. avium* 25291 to study the vascularization of the granuloma. The results obtained showed that small and medium sized granulomas were well vascularized but in advanced lesions blood vessels were only found at the periphery of the granulomas, as already published (48). It is therefore possible that the center of large granulomas become hypoxic due to this reduction in blood supply leading to the death of the cells further away from the blood vessels, i.e. macrophages within the deep core of the granuloma. However, it is known that macrophages can adapt to low oxygen tensions found in inflammatory sites (49, 50). This adaptation, as in most cells, involves the regulation of metabolic pathways controlled by the HIF system. To clarify a possible role of hypoxia in the development of necrotic granulomas in mycobacterial infections we studied the influence of HIF-1α in the development of necrosis of *M. avium*-induced granulomas. Total HIF-1α protein increased in liver mononuclear cells at 60 days of infection, a time-point where reduced vascularization of the granulomas was observed. Mice defective in myeloid HIF-1α developed earlier granuloma necrosis as compared to wild type WT animals, suggesting that HIF-1α is required for

405 cell survival within the granuloma and thus those cells at the core of these lesions may
406 be subjected to severe hypoxia. The cell death involved caspase-3 activation and
407 inter-nucleosomal DNA nicking suggesting that necrosis is secondary to apoptosis.
408 The accelerated granuloma necrosis preceded an increase of the bacterial growth
409 suggesting that mycobacterial control is not affected by the lack of HIF-1α as long as
410 the cells remain viable. This interpretation is supported by the fact that 1) HIF-1α-
411 deficient mice are as resistant to a low virulence *M. avium* strain as the WT mice
412 (unpublished observations); 2) no phenotype was observed in HIF-1α-deficient mice
413 infected with a high dose of *M. avium* 25291 where no necrosis of granulomas ever
414 occurs (unpublished data); 3) no major defects in the adaptive immune response were
415 found except for the increase in the accumulation of phagocytes likely a consequence
416 of the tissue damage and consequent exacerbation of the inflammation. Therefore, we
417 propose, that the increase in bacterial loads in the late time-points of infection, is the
418 result of the death of the host cells in granulomas undergoing necrosis. Although
419 factors other than hypoxia may regulate the expression of this transcription factor
420 either at the transcriptional or post-translational levels, such as IFN-γ and LPS (51),
421 we found similar expression of IFN-γ (52, 53) and only minor changes in T cell
422 populations. HIF-1α is involved in the regulation of transcription in activated
423 macrophages namely of iNOS (51). Although NO is not participating in the IFN-γ-
424 induced control of *M. avium* growth, HIF-1α could possibly be required for the
425 expression of additional antimicrobial systems. In fact, even under normoxia, HIF-1α
426 is induced by bacterial infection and regulated by TNF-α and IFN-γ (15, 27, 38).
427 However, we detected no macrophage defect in controlling *M. avium* proliferation *in*
428 *vitro* even upon cytokine activation of the cells. This study failed to provide evidence
429 of necrotic granulomas in the lung at the time-points analysed. This was likely due to

the small size of the lesions in an organ with a high oxygen tension. The formation of necrotic granulomas in the lung was achieved by Ehlers and colleagues by using a massive inoculum of a similar *M. avium* strain (10^5 CFU) following an aerosol inhalation and a long term infection (19 weeks) (54). Further work is being undertaken, studying longer time points of infection with bigger inocula in order to assess the role of granuloma volume and confluence and consequent hypoxia in the development of lung pathology.

Our data are consistent with the hypothesis that growing granulomas become progressively less vascularized, more hypoxic and eventually reach a state where the macrophages at the inner core of the lesion no longer survive the lack of oxygen and die. Such a sequence of events was here accelerated by depriving macrophages of the major adaptive system against hypoxia. As a consequence, cells died recruiting more phagocytes and bacteria found the appropriate ground for replication. The latter may not necessarily happen in an intact host where the oxygen tension reached within the necrotic granulomas would be expected to be much lower and likely restrictive of mycobacterial growth.-We propose that interfering with adaptation to hypoxia or reducing the growth of granulomas may provide ways to reduce pathology and prevent dissemination in mycobacterial infections.

Acknowledgements

This work received support from"NORTE-07-0124-FEDER-000002-Host-Pathogen Interactions" co-funded by *Programa Operacional Regional do Norte* (ON.2—O Novo Norte), under the *Quadro de Referência Estratégico Nacional* (QREN) and from FCT/MEC through national funds co-financed by FEDER, under the PT2020 Partnership Agreement. TMS receives a postdoctoral grant ON2201310 from"NORTE-07-0124-FEDER-000002-Host-Pathogen Interactions" co-funded by Programa Operacional Regional do Norte (ON.2—O Novo Norte), under the Quadro de Referência Estratégico Nacional (QREN). MR receives the PhD grant SFRH/BD/89871/2012 from FCT, Portugal. The authors acknowledge Eduardo S. Martins for his help in preliminary data collection.

References

1. **Orme IM, Basaraba RJ.** 2014. The formation of the granuloma in tuberculosis infection. Semin Immunol **26:**601-609.
2. **Orme IM.** 1998. The immunopathogenesis of tuberculosis: a new working hypothesis. Trends Microbiol **6:**94-97.
3. **Kondratieva E, Logunova N, Majorov K, Averbakh M, Apt A.** 2010. Host genetics in granuloma formation: human-like lung pathology in mice with reciprocal genetic susceptibility to M. tuberculosis and M. avium. PLoS One **5:**e10515.
4. **Harper J, Skerry C, Davis SL, Tasneen R, Weir M, Kramnik I, Bishai WR, Pomper MG, Nuermberger EL, Jain SK.** 2012. Mouse model of necrotic tuberculosis granulomas develops hypoxic lesions. J Infect Dis **205:**595-602.
5. **Heitmann L, Abad Dar M, Schreiber T, Erdmann H, Behrends J, Mckenzie AN, Brombacher F, Ehlers S, Hölscher C.** 2014. The IL-13/IL-4Rα axis is involved in tuberculosis-associated pathology. J Pathol **234:**338-350.
6. **Cooper AM, Dalton DK, Stewart TA, Griffin JP, Russell DG, Orme IM.** 1993. Disseminated tuberculosis in interferon gamma gene-disrupted mice. J Exp Med **178:**2243-2247.
7. **Flynn JL, Goldstein MM, Chan J, Triebold KJ, Pfeffer K, Lowenstein CJ, Schreiber R, Mak TW, Bloom BR.** 1995. Tumor necrosis factor-alpha is required in the protective immune response against Mycobacterium tuberculosis in mice. Immunity **2:**561-572.
8. **Chiu CP, Wong WW, Kuo B, Tiao TM, Fung CP, Liu CY.** 1999. Clinical analysis of Mycobacterium tuberculosis infection in patients with acquired immunodeficiency syndrome. J Microbiol Immunol Infect **32:**250-256.
9. **Flórido M, Cooper AM, Appelberg R.** 2002. Immunological basis of the development of necrotic lesions following Mycobacterium avium infection. Immunology **106:**590-601.
10. **Borges M, Rosa GT, Appelberg R.** 2011. The death-promoting molecule tumour necrosis factor-related apoptosis inducing ligand (TRAIL) is not required for the development of peripheral lymphopenia or granuloma necrosis during infection with virulent Mycobacterium avium. Clin Exp Immunol **164:**407-416.
11. **Flórido M, Appelberg R.** 2004. Granuloma necrosis during Mycobacterium avium infection does not require tumor necrosis factor. Infect Immun **72:**6139-6141.
12. **Flórido M, Appelberg R.** 2006. Genetic control of immune-mediated necrosis of Mycobacterium avium granulomas. Immunology **118:**122-130.
13. **Flórido M, Pearl JE, Solache A, Borges M, Haynes L, Cooper AM, Appelberg R.** 2005. Gamma interferon-induced T-cell loss in virulent Mycobacterium avium infection. Infect Immun **73:**3577-3586.
14. **Roiniotis J, Dinh H, Masendycz P, Turner A, Elsegood CL, Scholz GM, Hamilton JA.** 2009. Hypoxia prolongs monocyte/macrophage survival and enhanced glycolysis is associated with their maturation under aerobic conditions. J Immunol **182:**7974-7981.
15. **Pugh CW, Ratcliffe PJ.** 2003. Regulation of angiogenesis by hypoxia: role of the HIF system. Nat Med **9:**677-684.
16. **Haase VH.** 2013. Regulation of erythropoiesis by hypoxia-inducible factors. Blood Rev **27:**41-53.
17. **Corzo CA, Condamine T, Lu L, Cotter MJ, Youn JI, Cheng P, Cho HI, Celis E, Quiceno DG, Padhya T, McCaffrey TV, McCaffrey JC, Gabrilovich DI.** 2010. HIF-1α regulates

function and differentiation of myeloid-derived suppressor cells in the tumor microenvironment. J Exp Med **207:**2439-2453.

18. **Greijer AE, van der Wall E.** 2004. The role of hypoxia inducible factor 1 (HIF-1) in hypoxia induced apoptosis. J Clin Pathol **57:**1009-1014.
19. **Ke Q, Costa M.** 2006. Hypoxia-inducible factor-1 (HIF-1). Mol Pharmacol **70:**1469-1480.
20. **Weidemann A, Johnson RS.** 2008. Biology of HIF-1alpha. Cell Death Differ **15:**621-627.
21. **Shweiki D, Itin A, Soffer D, Keshet E.** 1992. Vascular endothelial growth factor induced by hypoxia may mediate hypoxia-initiated angiogenesis. Nature **359:**843-845.
22. **Hayashi M, Sakata M, Takeda T, Yamamoto T, Okamoto Y, Sawada K, Kimura A, Minekawa R, Tahara M, Tasaka K, Murata Y.** 2004. Induction of glucose transporter 1 expression through hypoxia-inducible factor 1alpha under hypoxic conditions in trophoblast-derived cells. J Endocrinol **183:**145-154.
23. **Tacchini L, Bianchi L, Bernelli-Zazzera A, Cairo G.** 1999. Transferrin receptor induction by hypoxia. HIF-1-mediated transcriptional activation and cell-specific post-transcriptional regulation. J Biol Chem **274:**24142-24146.
24. **Scholz CC, Taylor CT.** 2013. Targeting the HIF pathway in inflammation and immunity. Curr Opin Pharmacol **13:**646-653.
25. **Cramer T, Yamanishi Y, Clausen BE, Förster I, Pawlinski R, Mackman N, Haase VH, Jaenisch R, Corr M, Nizet V, Firestein GS, Gerber HP, Ferrara N, Johnson RS.** 2003. HIF-1alpha is essential for myeloid cell-mediated inflammation. Cell **112:**645-657.
26. **Anand RJ, Gribar SC, Li J, Kohler JW, Branca MF, Dubowski T, Sodhi CP, Hackam DJ.** 2007. Hypoxia causes an increase in phagocytosis by macrophages in a HIF-1alpha-dependent manner. J Leukoc Biol **82:**1257-1265.
27. **Peyssonnaux C, Datta V, Cramer T, Doedens A, Theodorakis EA, Gallo RL, Hurtado-Ziola N, Nizet V, Johnson RS.** 2005. HIF-1alpha expression regulates the bactericidal capacity of phagocytes. J Clin Invest **115:**1806-1815.
28. **Thiel M, Caldwell CC, Kreth S, Kuboki S, Chen P, Smith P, Ohta A, Lentsch AB, Lukashev D, Sitkovsky MV.** 2007. Targeted deletion of HIF-1alpha gene in T cells prevents their inhibition in hypoxic inflamed tissues and improves septic mice survival. PLoS One **2:**e853.
29. **Kojima H, Gu H, Nomura S, Caldwell CC, Kobata T, Carmeliet P, Semenza GL, Sitkovsky MV.** 2002. Abnormal B lymphocyte development and autoimmunity in hypoxia-inducible factor 1alpha -deficient chimeric mice. Proc Natl Acad Sci U S A **99:**2170-2174.
30. **Walmsley SR, Print C, Farahi N, Peyssonnaux C, Johnson RS, Cramer T, Sobolewski A, Condliffe AM, Cowburn AS, Johnson N, Chilvers ER.** 2005. Hypoxia-induced neutrophil survival is mediated by HIF-1alpha-dependent NF-kappaB activity. J Exp Med **201:**105-115.
31. **Köhler T, Reizis B, Johnson RS, Weighardt H, Förster I.** 2012. Influence of hypoxia-inducible factor 1α on dendritic cell differentiation and migration. Eur J Immunol **42:**1226-1236.
32. **Jantsch J, Chakravortty D, Turza N, Prechtel AT, Buchholz B, Gerlach RG, Volke M, Gläsner J, Warnecke C, Wiesener MS, Eckardt KU, Steinkasserer A, Hensel M, Willam C.** 2008. Hypoxia and hypoxia-inducible factor-1 alpha modulate lipopolysaccharide-induced dendritic cell activation and function. J Immunol **180:**4697-4705.
33. **Dang EV, Barbi J, Yang HY, Jinasena D, Yu H, Zheng Y, Bordman Z, Fu J, Kim Y, Yen HR, Luo W, Zeller K, Shimoda L, Topalian SL, Semenza GL, Dang CV, Pardoll DM,**

Pan F. 2011. Control of T(H)17/T(reg) balance by hypoxia-inducible factor 1. Cell **146:**772-784.

34. **Shi LZ, Wang R, Huang G, Vogel P, Neale G, Green DR, Chi H.** 2011. HIF1alpha-dependent glycolytic pathway orchestrates a metabolic checkpoint for the differentiation of TH17 and Treg cells. J Exp Med **208:**1367-1376.

35. **Isoe T, Makino Y, Mizumoto K, Sakagami H, Fujita Y, Honjo J, Takiyama Y, Itoh H, Haneda M.** 2010. High glucose activates HIF-1-mediated signal transduction in glomerular mesangial cells through a carbohydrate response element binding protein. Kidney Int **78:**48-59.

36. **Blouin CC, Pagé EL, Soucy GM, Richard DE.** 2004. Hypoxic gene activation by lipopolysaccharide in macrophages: implication of hypoxia-inducible factor 1alpha. Blood **103:**1124-1130.

37. **Der SD, Zhou A, Williams BR, Silverman RH.** 1998. Identification of genes differentially regulated by interferon alpha, beta, or gamma using oligonucleotide arrays. Proc Natl Acad Sci U S A **95:**15623-15628.

38. **Zhou J, Schmid T, Brüne B.** 2003. Tumor necrosis factor-alpha causes accumulation of a ubiquitinated form of hypoxia inducible factor-1alpha through a nuclear factor-kappaB-dependent pathway. Mol Biol Cell **14:**2216-2225.

39. **van Uden P, Kenneth NS, Rocha S.** 2008. Regulation of hypoxia-inducible factor-1alpha by NF-kappaB. Biochem J **412:**477-484.

40. **Flórido M, Gonçalves AS, Silva RA, Ehlers S, Cooper AM, Appelberg R.** 1999. Resistance of virulent Mycobacterium avium to gamma interferon-mediated antimicrobial activity suggests additional signals for induction of mycobacteriostasis. Infect Immun **67:**3610-3618.

41. **Gomes MS, Appelberg R.** 2002. NRAMP1- or cytokine-induced bacteriostasis of Mycobacterium avium by mouse macrophages is independent of the respiratory burst. Microbiology **148:**3155-3160.

42. **Gordon S, Lawson L, Rabinowitz S, Crocker PR, Morris L, Perry VH.** 1992. Antigen markers of macrophage differentiation in murine tissues. Curr Top Microbiol Immunol **181:**1-37.

43. **Aly S, Wagner K, Keller C, Malm S, Malzan A, Brandau S, Bange FC, Ehlers S.** 2006. Oxygen status of lung granulomas in Mycobacterium tuberculosis-infected mice. J Pathol **210:**298-305.

44. **Kuhn A, Brachtendorf G, Kurth F, Sonntag M, Samulowitz U, Metze D, Vestweber D.** 2002. Expression of endomucin, a novel endothelial sialomucin, in normal and diseased human skin. J Invest Dermatol **119:**1388-1393.

45. **Via LE, Lin PL, Ray SM, Carrillo J, Allen SS, Eum SY, Taylor K, Klein E, Manjunatha U, Gonzales J, Lee EG, Park SK, Raleigh JA, Cho SN, McMurray DN, Flynn JL, Barry CE.** 2008. Tuberculous granulomas are hypoxic in guinea pigs, rabbits, and nonhuman primates. Infect Immun **76:**2333-2340.

46. **Benini J, Ehlers EM, Ehlers S.** 1999. Different types of pulmonary granuloma necrosis in immunocompetent vs. TNFRp55-gene-deficient mice aerogenically infected with highly virulent Mycobacterium avium. J Pathol **189:**127-137.

47. **Pearl JE, Saunders B, Ehlers S, Orme IM, Cooper AM.** 2001. Inflammation and lymphocyte activation during mycobacterial infection in the interferon-gamma-deficient mouse. Cell Immunol **211:**43-50.

48. **Aly S, Laskay T, Mages J, Malzan A, Lang R, Ehlers S.** 2007. Interferon-gamma-dependent mechanisms of mycobacteria-induced pulmonary immunopathology: the role of angiostasis and CXCR3-targeted chemokines for granuloma necrosis. J Pathol **212:**295-305.

49. **Riboldi E, Porta C, Morlacchi S, Viola A, Mantovani A, Sica A.** 2013. Hypoxia-mediated regulation of macrophage functions in pathophysiology. Int Immunol **25:**67-75.

50. **Strehl C, Fangradt M, Fearon U, Gaber T, Buttgereit F, Veale DJ.** 2014. Hypoxia: how does the monocyte-macrophage system respond to changes in oxygen availability? J Leukoc Biol **95:**233-241.

51. **Takeda N, O'Dea EL, Doedens A, Kim JW, Weidemann A, Stockmann C, Asagiri M, Simon MC, Hoffmann A, Johnson RS.** 2010. Differential activation and antagonistic function of HIF-{alpha} isoforms in macrophages are essential for NO homeostasis. Genes Dev **24:**491-501.

52. **Appelberg R, Castro AG, Pedrosa J, Silva RA, Orme IM, Minóprio P.** 1994. Role of gamma interferon and tumor necrosis factor alpha during T-cell-independent and -dependent phases of Mycobacterium avium infection. Infect Immun **62:**3962-3971.

53. **Saunders BM, Cheers C.** 1995. Inflammatory response following intranasal infection with Mycobacterium avium complex: role of T-cell subsets and gamma interferon. Infect Immun **63:**2282-2287.

54. **Ehlers S, Benini J, Held HD, Roeck C, Alber G, Uhlig S.** 2001. Alphabeta T cell receptor-positive cells and interferon-gamma, but not inducible nitric oxide synthase, are critical for granuloma necrosis in a mouse model of mycobacteria-induced pulmonary immunopathology. J Exp Med **194:**1847-1859.

Figure Legends

Figure 1. Immunohistochemical staining of F4/80-positive cells in liver sections from WT mice infected with *M. avium* 25291 for (A) 30 days, (B) 60 days, (C) 90 days, and (D) 120 days.

Figure 2. Immunohistochemical staining of endomucin-positive cells in liver sections from WT mice infected with *M. avium* 25291 for (A) 90 days and (B-D) 120 days.

Figure 3. HIF-1α accumulates and its absence increases the susceptibility to *M. avium* 25291 infection. (A) Analysis of total HIF-1α protein in liver mononuclear cells during *M. avium* infection. Groups of non-infected mice (day 0) were included at every time-point of infection studied. Each group of non-infected mice comprised three to four animals and each group of infected mice comprised four to six animals. Data are expressed as mean + SD of protein levels calculated from the total liver mononuclear cells for individual mice. ** $p<0.01$, *** $p<0.001$ comparing values from infected and non-infected animals. (B, C) Representative photographs of spleens and livers respectively, from infected mice at day 96 post-infection. (D) Representative kinetics of 25291 *M. avium* infection of the liver and spleen from WT and HIF-1α$^{-/-}$ mice. Data represent the mean and SD of CFU from five mice per group of one of three experiments.*$p<0.05$, **$p<0.01$, ***$p<0.001$ (stastically significant differences between WT and HIF-1α$^{-/-}$mice).

Figure 4. Myeloid ablation of HIF-1α influences granuloma progression during *M. avium* infection. (A, C, E) Representative lesions in liver sections from infected WT

mice. (B, D, F) Representative lesions in liver sections from infected HIF-1$\alpha^{-/-}$ mice. (A, B) 30 days, (C, D) 60 days, and (E, F) 104 days post-infection. (G) Percentage of infiltrated area for WT and HIF-1$\alpha^{-/-}$ mice.***p<0.001 comparing total percentage infiltrated area of WT *versus* HIF-1$\alpha^{-/-}$ mice. +p<0.05 comparing necrotic with non-necrotic area of HIF-1$\alpha^{-/-}$ mice. (H) Number of cellular infiltrates for WT (closed bars) and HIF-1$\alpha^{-/-}$(open bars) mice. Data are expressed as mean+ SD of the areas from mice analyzed individually in each group. ***p<0.001 comparing WT with HIF-1$\alpha^{-/-}$ mice.

Figure 5. Evidence of apoptotic cell death within the granulomas of HIF-1$\alpha^{-/-}$ mice. A representative lesion from a HIF-1$\alpha^{-/-}$ mouse infected for 104 days is shown. Tissue sections of liver tissue were analysed by performing the immunodetection of cleaved caspase-3 and the TUNEL assay (green fluorescence). Nuclei were stained blue by DAPI. C and D are magnifications of the inserts shown in A and B, respectively.

Figure 6. *M. avium*-infected HIF-1$\alpha^{-/-}$ present increased numbers of mononuclear cells at late time-points of infection. Cellular composition of spleens (A) and livers (B) from WT and HIF-1$\alpha^{-/-}$ mice. Groups of non-infected mice (day 0) were included at every time-point of infection studied. Each group comprised 5 animals. All data are expressed as mean + SD of one of three experiments. *p<0.05, **p<0.01, ***p<0.001, comparing infected WT with HIF-1$\alpha^{-/-}$ mice. +p<0.05, ++p<0.01, +++p<0.001 comparing infected *versus* non-infected (day 0) animals.

Figure 1

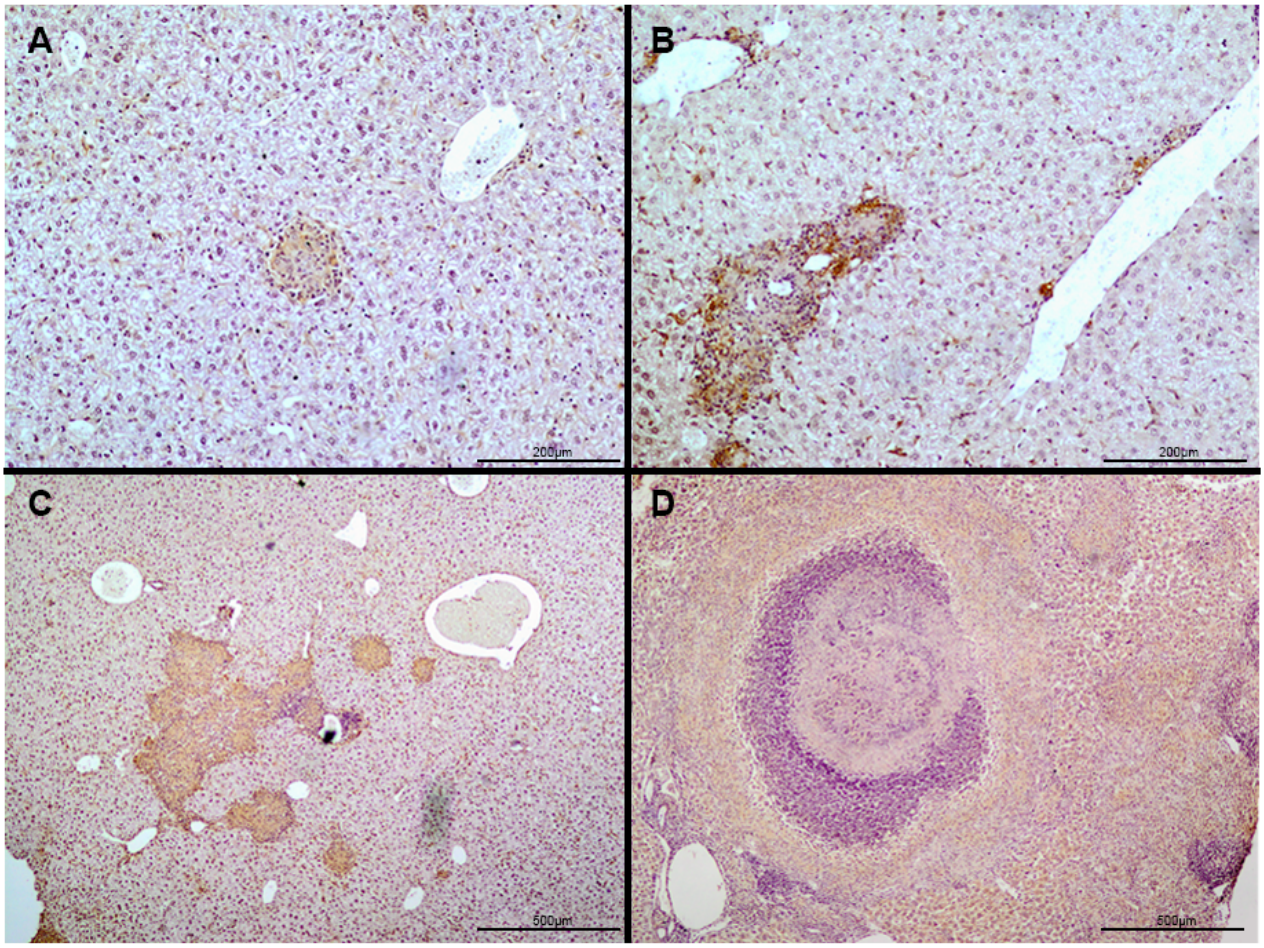

Figure 2

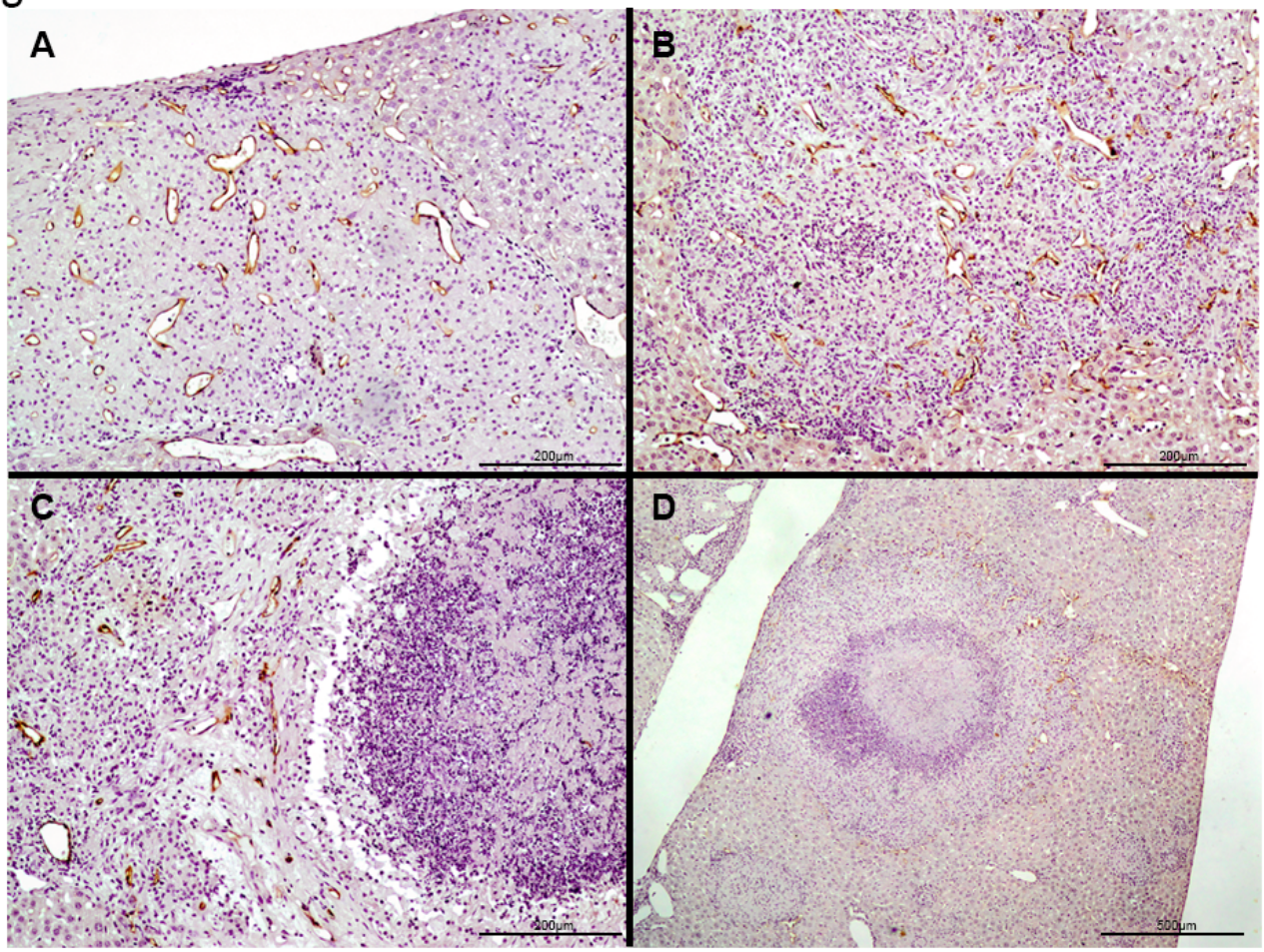

Figure 3

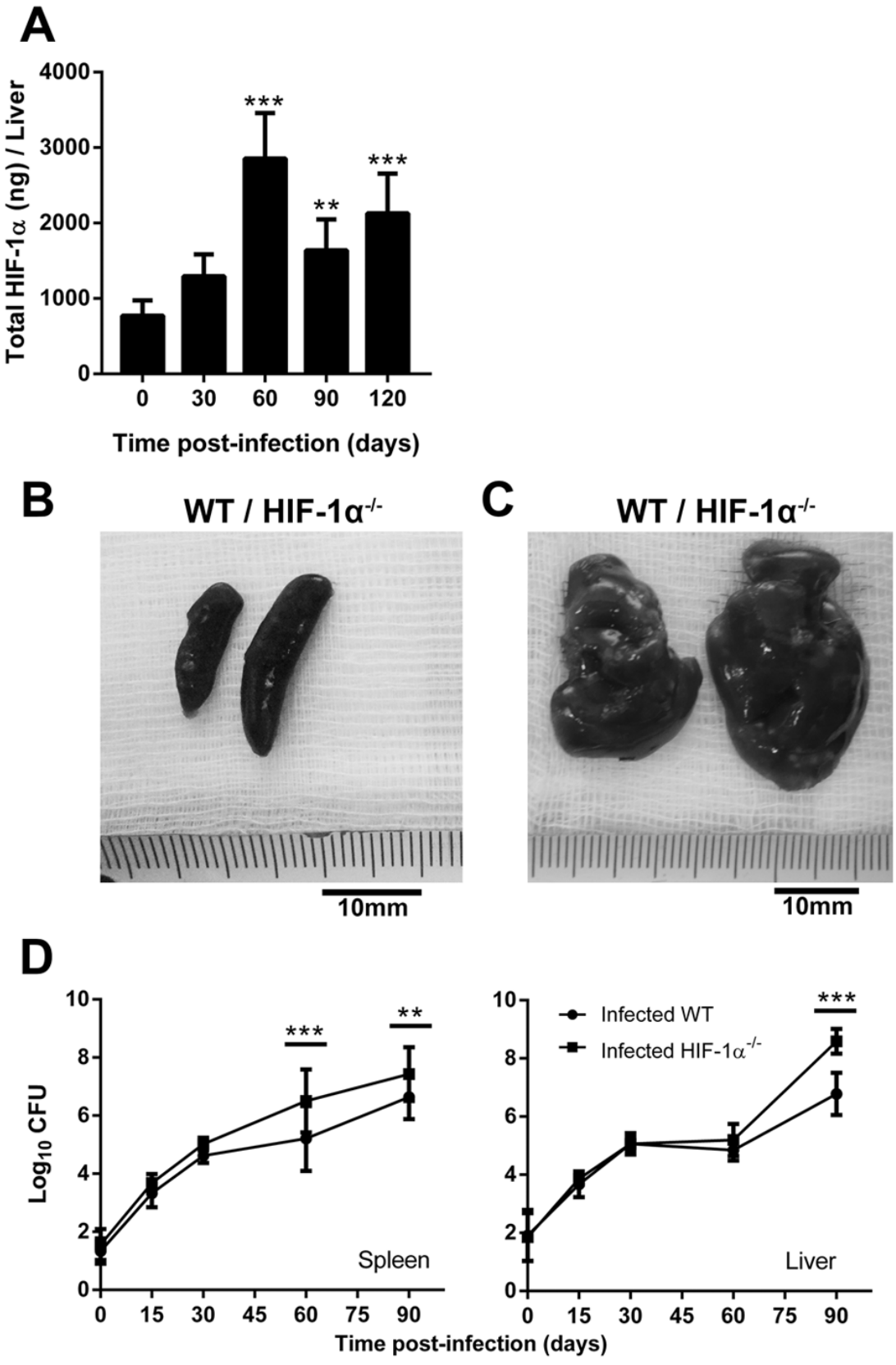

Figure 4

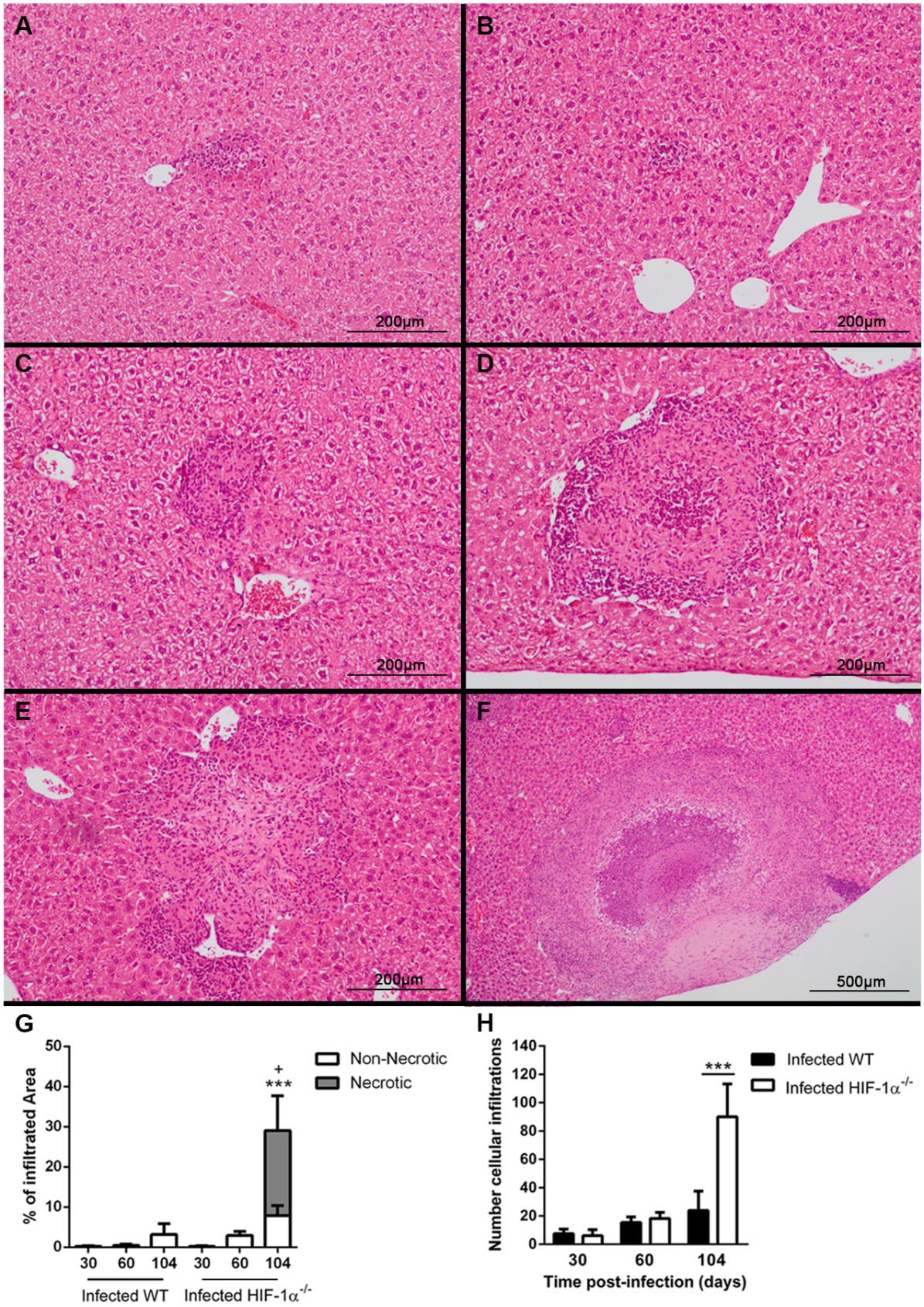

Figure 5

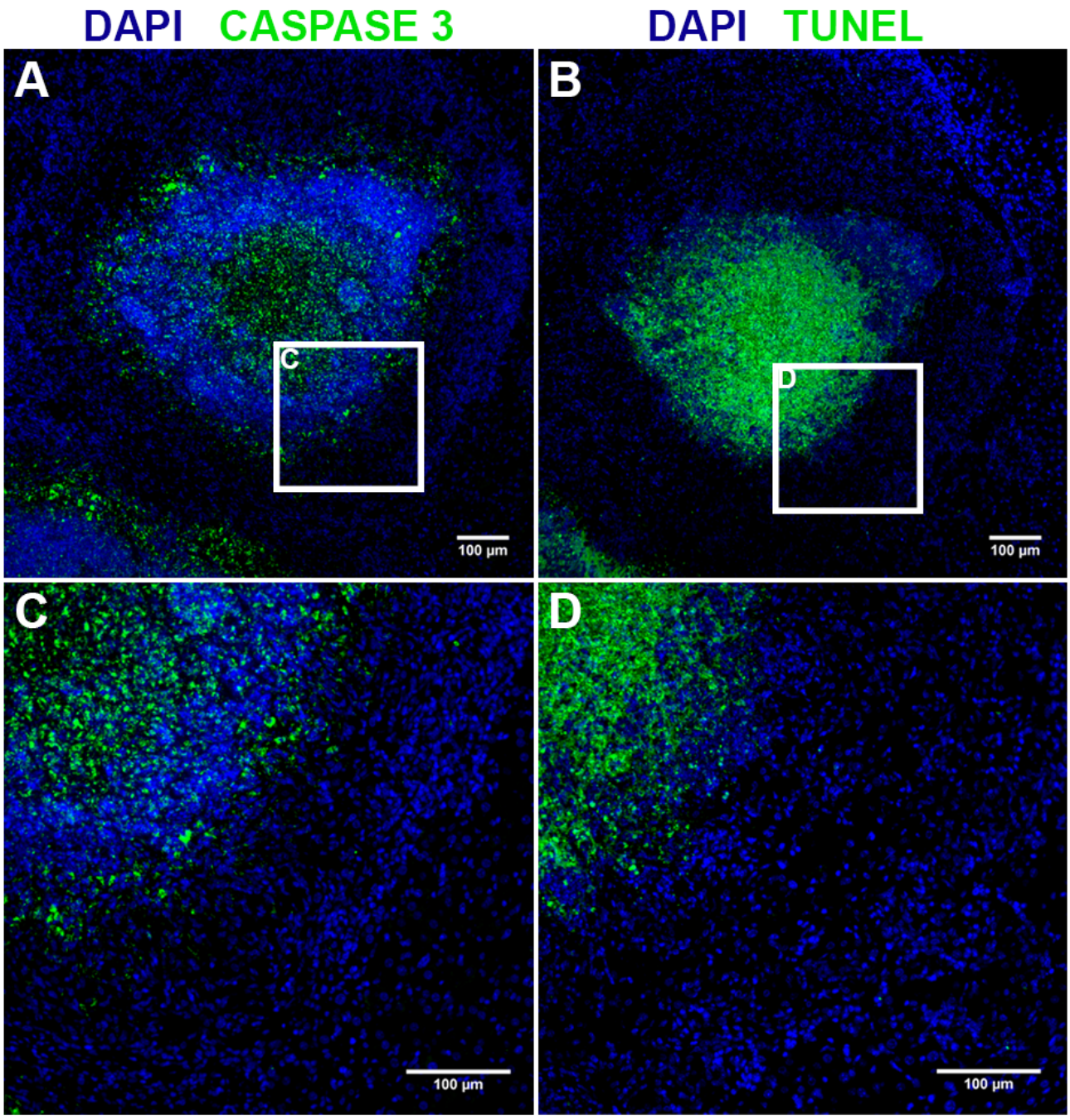

Figure 6